MODELS OF SPECTRAL RADIATION HEAT TRANSFER FOR MARTIAN SPACE VEHICLES

Andrienko Daniil[1,2], Surzhikov Sergey[1]

[1] Moscow Institute of Physics and technology,141700, Russia, Moscow region, Dolgoprudnii, Institutski per. 9, Email: daniilandrienko@gmail.com

[2] Institute for Problems in Mechanics RAS,119526, Russia, Moscow, prosp. Vernadskogo 101, bl.1, Email: surg@ipmnet.ru

ABSTRACT

Actual problems of space science, gasdynamics and plasma physics requires the registration of radiative heat transfer for more accurate calculation thermal characteristics modeling objects. Through the huge amount of methods it is possible to distinguish the spherical harmonics method (SHM) which is quite simple for computer implementation. [1]-[5], [9]. It is possible to calculate the volume heat generation and radiative flux to the surface using SHM.

This work is dedicated to resolving the heat transfer equation in P_1-approximation of SHM in complex geometry under assumption of nonscattering media. Besides benefits of the P_1-approximation of SHM there are few of lacks, which were discussed in [1], [2], [4], [9]. Among of this lacks one can distinguish the unsatisfied accuracy of SHM near boundaries and under relative small absorption of radiation. But, despite of this lacks, there are weighty arguments of applying the P_1-approximation of SHM. This is the main reason of future investigation of the P_1-approximation of SHM respectively to the number of physical mechanic problems.

1. THE GEOMETRY OF THE PROBLEM

1.1 The flat geometry mesh

On fig. 1 the geometry, used for computation transfer of high temperature gas radiation within flat layer is shown. This type of geometry is chosen because of presence of analytical solution of one dimensional heat transfer problem along the axis of symmetry far from edges. The number of nodes along axis z and r is equal to 50 and 250 respectively. The grid, depicted on fig. 1 is regular, uniform and orthogonal. Such relative grid simplicity let us exclude the influence of discretization procedure, topology of the mesh and focus on the principal difference between the P_1-approximation of SHM and analytical solution.

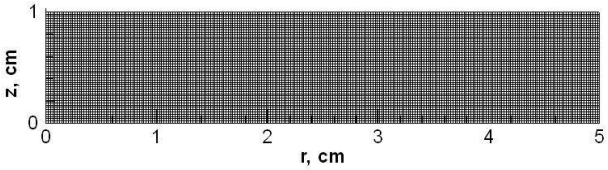

Fig. 1. Structured grid for calculation radiative heat transfer within the flat layer.

1.2 The complex geometry mesh

On fig. 2 the mesh, used for calculating heat transfer within the complex geometry is presented. Because of axisymmetric problem statement, computations are carried out only for the upper half of computational domain, restricted with the equation y=0. The number of nodes is equal to 141x61 along the spherical boundaries and axis of symmetry respectively. The mesh refinement in the domain of the most gradients is made analytically, for details see [8].

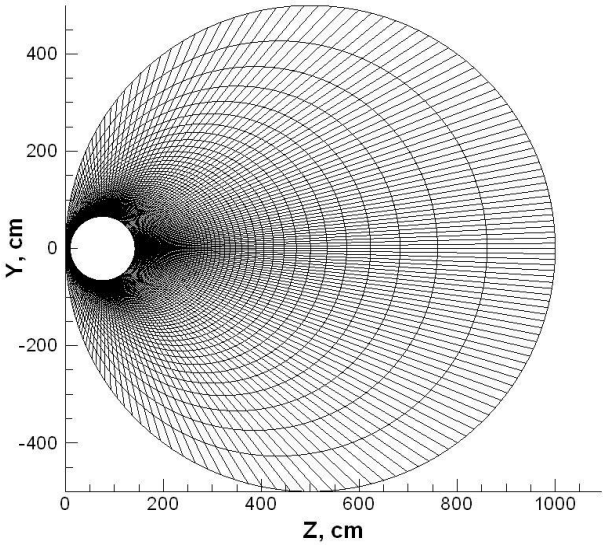

Fig. 2. Structured grid in the neighbourhood of spherical body, number of nodes is 141x61

2. GOVERNING SYSTEM OF EQUATIONS

The spectral intensity of radiation satisfies the unsteady equation of heat transfer:

$$\frac{1}{c}\frac{\partial J_\nu\ s,\Omega,t}{\partial t}+\frac{\partial J_\nu\ s,\Omega,t}{\partial s}+ \\ +\left[\kappa_\nu\ s,t\ +\sigma_\nu\ s,t\ \right]J_\nu\ s,\Omega,t\ = \\ =J_\nu^{em}\ s,t\ +\frac{1}{4\pi}\sigma_\nu\ s,t\ \cdot \\ \int_{\nu'=0}^{\infty}\int_{\Omega'=4\pi}\gamma\ s,\Omega,\Omega',\nu',\nu\ J_{\nu'}\ s,\Omega',t\ d\Omega' d\nu', \tag{1}$$

where t - time, c - light velocity, $J_\nu(s,\Omega)$ - spectral intensity of radiation, ν - the frequency of radiation, s - spatial coordinate along the ray, Ω - unit vector directions, $\kappa_\nu\ s$ - the volume spectral coefficient of absorption, $J_\nu^{em}\ s$ - unit volume spectral radiation ability, $\gamma\ s,\Omega,\Omega',\nu',\nu$ -the spectral scattering indicatrix, dependent from frequency and direction.

The approximation of local thermodynamic equilibrium is used for Eq. 1, which means that $J_\nu^{em}\ s\ =\kappa_\nu\ s\ J_{b,\nu}\ T\ s\ $, where $J_{b,\nu}\ T\ s\ $ - spectral intensity of black body. The media is considered nonscattering, i.e. $\sigma_\nu\ s,t\ =0$. Eq. 1 is considered to be quasisteady: the time-derivative summand $\frac{1}{c}\frac{\partial J_\nu\ s,\Omega,t}{\partial t}$ has a fictitious sense. This assumption is made for scheme established realization. Finally, Eq. 1 can be rewritten as

$$\frac{1}{c}\frac{\partial J_\nu\ s,\Omega,t}{\partial t}+\frac{\partial J_\nu\ s,\Omega,t}{\partial s}+ \\ +\kappa_\nu\ s\ J_\nu\ s,\Omega,t\ =\kappa_\nu\ s\ J_{b,\nu}\ s\ . \tag{2}$$

The P_1-approximation of SHM concludes in intensity of radiation series expansion into linear combination of orthogonal Legendre polynomials with the coefficients, depend on spatial coordinate. For details see [1]-[3], [6]. The integrating over the whole solid angle results in governing system of equations:

$$\frac{1}{c}\frac{\partial U}{\partial t}+\frac{1}{r}\frac{\partial rW_r}{\partial r}+\frac{\partial W_z}{\partial z}+\kappa_\nu cU=4\pi\kappa_\nu J_b, \tag{3}$$

$$\frac{c}{3\kappa_\nu}\frac{\partial U}{\partial r}+W_r=0, \tag{4}$$

$$\frac{c}{3\kappa_\nu}\frac{\partial U}{\partial z}+W_z=0, \tag{5}$$

where r,z – axis of cylindrical system of coordinates, W_r,W_z - radiation flux density projections, U - volume density of radiation, κ_ν - spectral coefficient of absorption, The spatial dependence in Eq. 3- 5 is omitted due to short.

Eq. 3-5 is equal to single equation with partial derivatives:

$$\frac{1}{r}\frac{\partial}{\partial r}(D_\nu r\frac{\partial U_\nu}{\partial r})+\frac{\partial}{\partial z}(D_\nu\frac{\partial U_\nu}{\partial z})+\kappa_\nu cU_\nu=\kappa_\nu cU_{b\nu}, \tag{6}$$

where $D_\nu=c/3\kappa_\nu$ - spectral diffusion coefficient.

As mentioned above, the structured meshes are used in this work because of more rapid convergence of iteration process (*references*) comparing with unstructured meshes. in addition, the finite element way of discretization is much more simple comparing with finite-volume way of discretization, for example.

Because of multi-block grid orientation, it is preferable to orthgonolize computational domain and mesh for simplifying mathematical calculations, for example, "stitching" the solution on the domain boundary. For this purpose a changing of coordinates is performed.

The cylindrical coordinates (r,z) is changed on curvilinear coordinates (ξ,η). Jacobean matrix J is not equal zero at any point of computational domain. The resulting equation in coordinates (ξ,η) has appearance

$$\frac{\partial}{\partial\xi}\left(\frac{D(\xi_r{}^2+\xi_z{}^2)}{J}\frac{\partial U}{\partial\xi}\right)+\frac{\partial}{\partial\eta}\left(\frac{D(\eta_r{}^2+\eta_z{}^2)}{J}\frac{\partial U}{\partial\eta}\right)+ \\ +\frac{\partial}{\partial\xi}\left(\frac{D(\xi_r\eta_r+\xi_z\eta_z)}{J}\frac{\partial U}{\partial\eta}\right)+ \\ +\frac{\partial}{\partial\eta}\left(\frac{D(\xi_r\eta_r+\xi_z\eta_z)}{J}\frac{\partial U}{\partial\xi}\right)+ \\ +\frac{1}{r}\left(\frac{D\xi_r}{J}\frac{\partial U}{\partial\xi}+\frac{D\eta_r}{J}\frac{\partial U}{\partial\eta}\right)+c\kappa U=c\kappa U_b, \tag{7}$$

In Eq. 7 the spectral index near D, U and κ is omitted for short.

3. BOUNDARY CONDITIONS

For Eq. 1 boundary conditions are formulated relatively the intensity of radiation:

$$x=0,0\le\mu\le1:\ J\ x=0,\mu\ =J_0^+$$
$$x=H,-1\le\mu\le0:\ J\ x=H,\mu\ =J_H^-,$$

but, because of postulation the relation between volume density of radiation and radiation flux density,

boundary conditions should be formulated relatively this variables. In this work the Marshak boundary conditions are used [3]:

$$W\ \ \tau = 0\ \ = -\frac{c}{3\kappa}\frac{dU}{dx}\bigg|_{\tau=0} = 2\pi J^{+}_{\tau=0} - \frac{c}{2}U\big|_{\tau=0},$$

$$W\ \ \tau = H\ \ = -\frac{c}{3\kappa}\frac{dU}{dx}\bigg|_{\tau=H} = -2\pi J^{-}_{\tau=H} + \frac{c}{2}U\big|_{\tau=H},$$

where τ - optical thick of medium layer along unit boundary normal. For our task optical length $\tau = 0$ is considered for boundary, adjacent to spherical body, and $\tau = H$ on the boundary, adjacent to unperturbed media. $J^{+}_{\tau=0}$ и $J^{-}_{\tau=H}$ - external intensity of radiation relatively to the computational domain, $J^{+}_{\tau=0} = J^{-}_{\tau=H} = 0$, are considered subsequently, so boundary conditions transforms to

$$-\frac{c}{3\kappa}\frac{dU}{dn}\bigg|_{\tau=0} = -\frac{c}{2}U\big|_{\tau=0}, \qquad (8)$$

$$-\frac{c}{3\kappa}\frac{dU}{dn}\bigg|_{\tau=H} = \frac{c}{2}U\big|_{\tau=H}. \qquad (9)$$

Eq. 8 and 9 have simple physical meaning: the radiative flux density to the domain boundary are equal diffuse component of radiation. Such type of boundary condition is approximate: according to the definition of volume density of radiation $U = \frac{2\pi}{c}\int\limits_{\Omega=4\pi} J d\Omega$, i.e. for accurate calculation of boundary condition we need inextricable radiation intensity function, integrating the intensity of radiation function defined only in the half of solid angle can lead to inaccuracy of boundary condition. Numerical experiments, carried out in this paper, proved the adequately behavior of Eq. 8 and 9.

4. HEAT TRANSFER IN FLAT DOMAIN

One dimensional radiative heat transfer within the flat layer can be described with Chandrasekhar's functions [10]. In this work the elongated cylindrical geometry is chosen for describing one-dimensional problem (fig. 3). Neglecting with boundary effects, there is one dimensional problem along the axis of symmetry. In present work H=1 см, R=5 см. Along the axis of symmetry boundary condition has appearance $\frac{\partial U}{\partial r} = 0$.

Boundary conditions 8 and 9 are used for boundaries compound with equations $z = 0$ and $z = H$. Temperature field is shown on fig. 3. Number of nodes is equal to 500x100 along r and z axis respectively.

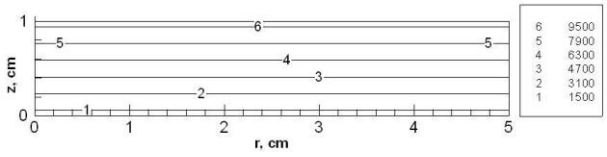

Fig. 3. Temperature distribution within the flat layer

Analytical solution for z-component of radiation density flux is described with expression:

$$W(\tau) = 2\pi\int\limits_{0}^{\tau} J_b\left[T\ \ \tau'\ \right]E_2\ \ \tau - \tau'\ \ d\tau' - 2\pi\int\limits_{\tau}^{\tau_H} J_b\left[T\ \ \tau'\ \right]E_2\ \ \tau' - \tau\ \ d\tau', \qquad (10)$$

where $E_n\ \ x\ = \int\limits_0^1 \exp\left(-\frac{x}{\mu}\right)\mu^{n-2} d\mu$ - Chandrasekhar's functions, $\tau = \int\limits_0^z \kappa dz'$ - optical thickness of media along z direction, $\tau_H = \int\limits_0^H \kappa dz$ - full optical thickness.

5. SPECTRAL MODEL OF HEAT TRANSFER IN COMPLEX DOMAIN

On the first step of numerical simulation the spectral absorption coefficient is considered to be equal constant value independently from the spatial coordinate and the frequency of radiation. The spectral intensity of radiation can be integrated over the whole spectral range under this approximation: $U_b = \tilde{\sigma}T^4/\pi$, where $\tilde{\sigma} = 5.67 erg/\ s\cdot cm^2\cdot K^4$ - Stefan-Boltzmann constant. Such approximation allows evaluate the volume density of radiation and flux density to the surface for a short period of time, avoiding the time-expensive spectral calculation. Further, the term *integral task of radiative heat transfer,* or, more shortly, *integral task,* will be applied for such kind of absorption coefficient approximation.

On the second step the dependence of absorption coefficient from pressure, temperature and chemical components concentration was taken into account. The gas-dynamic and chemical properties were calculated with program code NERAT 2D [3], the spectral properties were calculated with program code ASTEROID [11,12]. Further, the term spectral *task of radiative heat transfer,* or, more shortly, *spectral task,* will be applied for problem with real optical properties. The temperature, velocity, pressure fields and concentrations of gases mixture component, used for calculations in present work are presented on fig. 4-8.

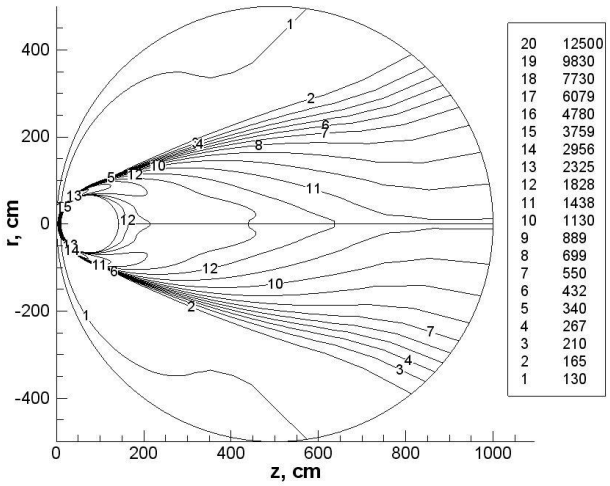

Fig. 4. Temperature field, K

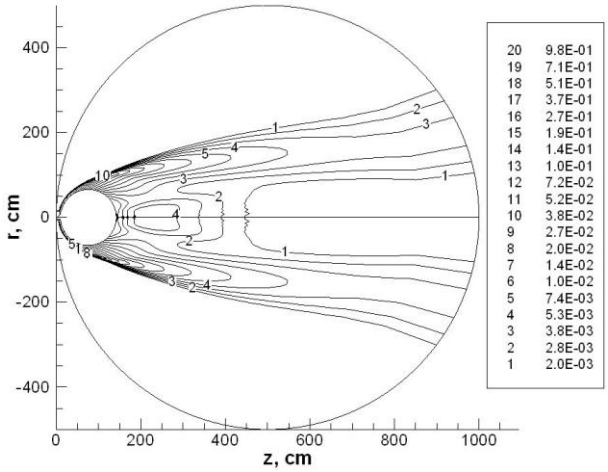

Fig. 5. Pressure field, atm.

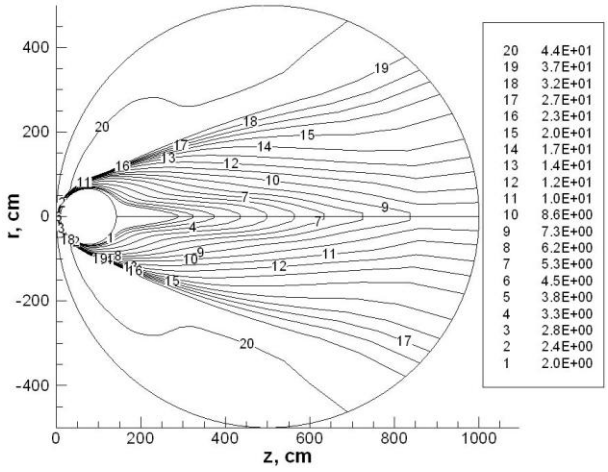

Fig. 6. Flow field on incident flux, M.

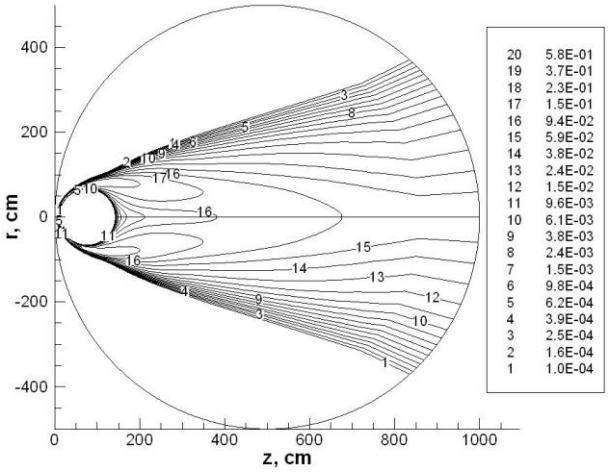

Fig. 7. Mass fraction of CO

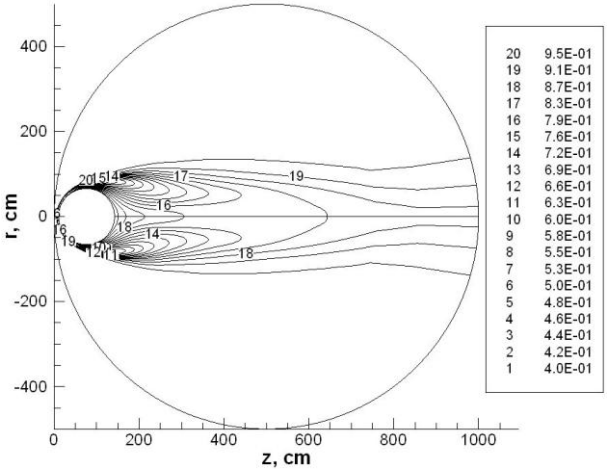

Fig. 8. Mass fraction of CO_2.

For a correct description of optical properties, the spectral range from low-frequency zone (10^3 cm^{-1}) up to high frequency zone (10^5 cm^{-1}) is divided into 90 spectral subranges, within every subrange the absorption coefficient is considered constant. As it was mentioned above, the full spectral problem is very time-expensive: the integral task has to be solved for each spectral group. The code optimization becomes crucial point.

On fig. 9 the maximum value of absorption coefficient within each spectral subrange is depicted. The dividing the whole spectral range on subranges is uniform. The boundaries of each spectral subrange are marked with triangles.

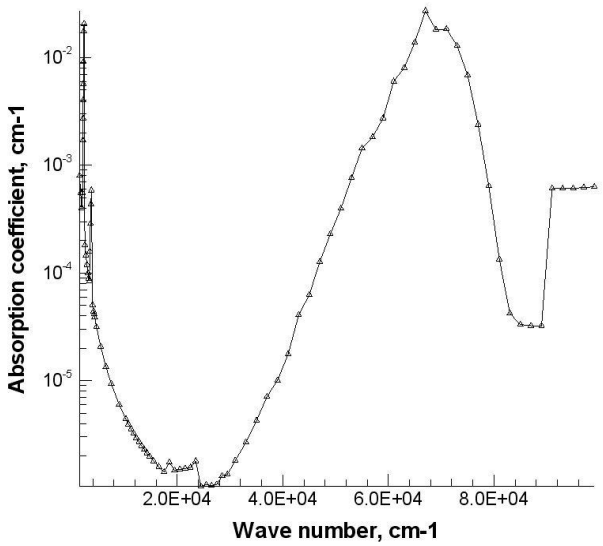

Fig. 9. The maximum of spectral absorption coefficient within each spectral subrange dependent from wave number for range $1.5\text{x}10^3$-10^5 cm^{-1}. The boundary of spectral groups marked with triangles.

Within each spectral subrange the spectral intensity of radiation is: $J^0_{b,\omega_0}\ T = \int_{\Delta\omega_g} J_{b,\omega}\ T\ d\omega$, where T - is temperature, K, ω_0 - wave number, h, k – Planks and Stephan-Boltzmann constants respectively. Spectral intensity in subrange $\omega_0 - \Delta\omega/2, \omega_0 + \Delta\omega/2$ is equal to $U_{\Delta\omega_g} = \kappa_g \int_{\Delta\omega_g} J_{b,\omega}\ T\ d\omega \approx \kappa_g J^0_{b,\Delta\omega_g}\ T$, where $\kappa_g = \frac{1}{\Delta\omega_g}\int_{\Delta\omega_g} \kappa_\omega d\omega$ - the coefficient of absorption within definite spectral subrange. The summation over all spectral subranges gives the integral volume density of radiation: $U = \sum_{g=1}^{N} U_{\Delta\omega_g}$.

6. RESULTS

6.1 The heat transfer in the flat layer

In this section the comparing of flux density of radiation, calculated through the P_1-approximation of SHM and analytical solution (Eq. 10) for flat layer (fig. 3) is made. Three numerical experiments is made: for absorption coefficient $\kappa = 10$ cm^{-1}, $\kappa = 1$ cm^{-1}, $\kappa = 0.1$ cm^{-1}, $\kappa = 0.01$ cm^{-1}, the appropriate distribution of flux density are presented on fig. 10-13.

At optical thick of radiative layer $\tau_H = 10$ (fig. 10) the flux density value, predicted by the P_1-approximation of SHM is in a good agreement with analytical solution (the relative difference is approximately 0.5%). While decreasing the optical thick the relative difference became greater. At $\tau_H = 1$ (fig. 11) the relative difference is equal to 23%, at $\tau_H = 0.1$ (fig. 12) - 11%, at $\tau_H = 0.01$ (fig. 13) - 13%.

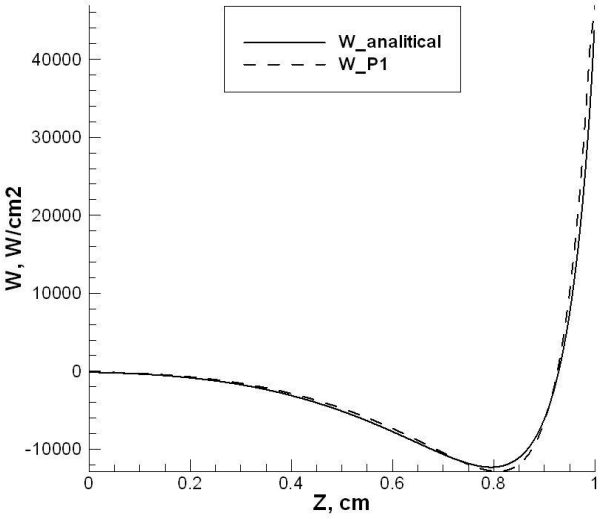

Fig. 10. Axial projection of density flux, W/cm^2, $\kappa = 10\text{cm}^{-1}$. The solid curve - P_1-approximation of SHM, the dashed curve – analytical solution.

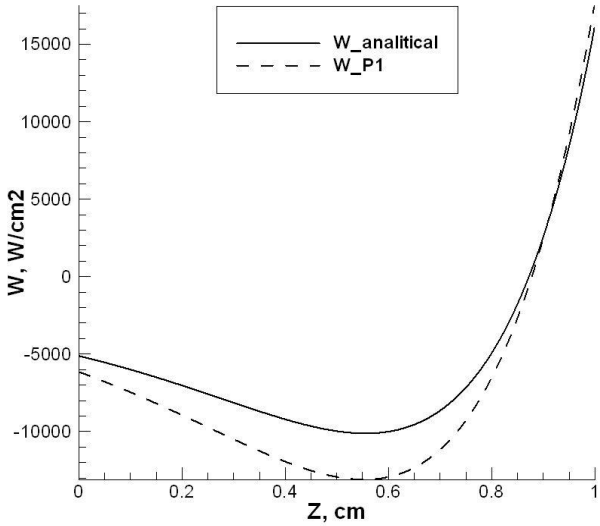

Fig. 11. Axial projection of density flux, W/cm^2, $\kappa = 1\text{cm}^{-1}$. The solid curve - P_1-approximation of SHM, the dashed curve – analytical solution.

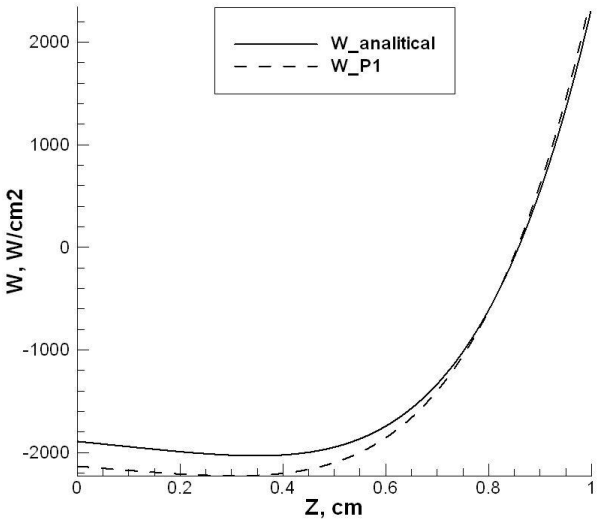

Fig. 12 Axial projection of density flux, W/cm^2, $\kappa = 0.1cm^{-1}$. The solid curve - P_1-approximation of SHM, the dashed curve – analytical solution.

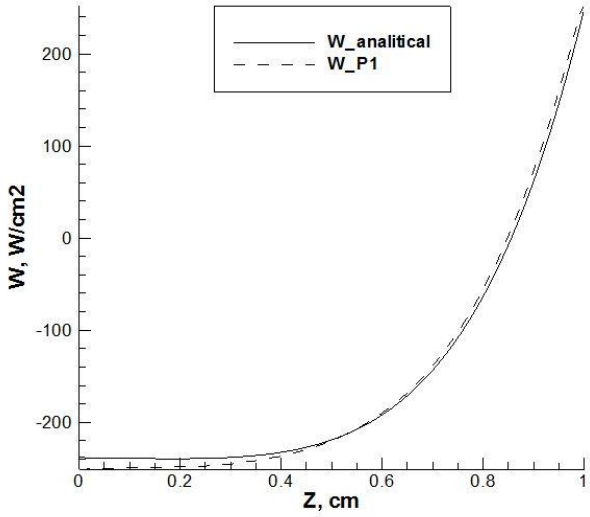

Fig. 13. Axial projection of density flux, W/cm^2, $\kappa = 0.01cm^{-1}$. The solid curve - P_1-approximation of SHM, the dashed curve – analytical solution.

6.2 Heat transfer in complex geometry

Each numerical experiment in integral task for the geometry type, depicted on fig. 2 the coefficient of absorption is considered to vary in range from 1 cm^{-1} up to 10^{-2} cm^{-1}. The flux density on the surface of spherical body, calculated through P_1-approximation and ray-tracing method (RTM, see [11]) is compared on fig. 14-16. The relative difference between SHM and RTM becomes greater with absorption coefficient decreasing.

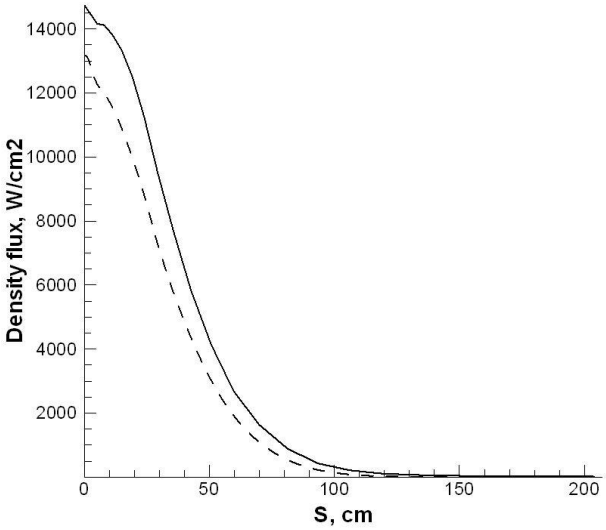

Fig. 14. The flux density to the spherical body, solid curve – RTM, dashed curve - P_1-approximation of SHM, $\kappa = 1cm^{-1}$.

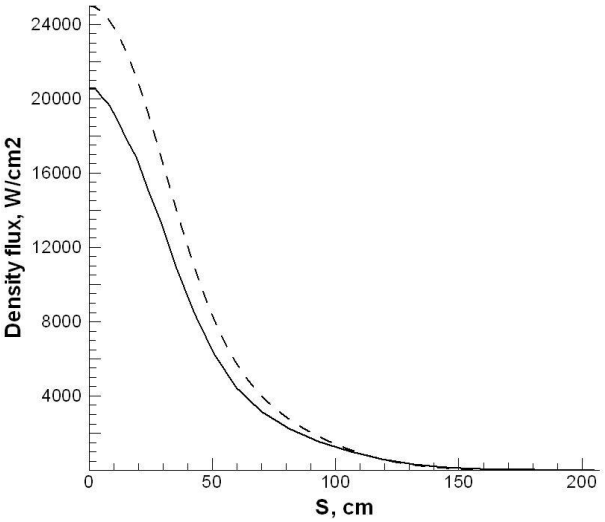

Fig. 15. The flux density to the spherical body, solid curve – RTM, dashed curve - P_1-approximation of SHM, $\kappa = 0.1cm^{-1}$.

Taking into account the fact, that relative contribution the spectral density flux at small absorption coefficient is sufficiently smaller than at optically thick media, one may conclude, that "cutting off" spectral groups with coefficient of absorption smaller than 0.01 cm^{-1} will not bring in great inaccuracy into resulting value of density flux. It is possible to see from fig. 9 that there is almost no absorption within the range 10^4 $cm^{-1} \le \nu \le 10^5$ cm^{-1}. In this work the spectral task of heat transfer was performed two numerical experiments: for 7 spectral groups among of 90 with the absorption coefficient greater than 10^{-2} cm^{-1} and for 17 groups with the absorption coefficient greater than 10^{-3} cm^{-1}.

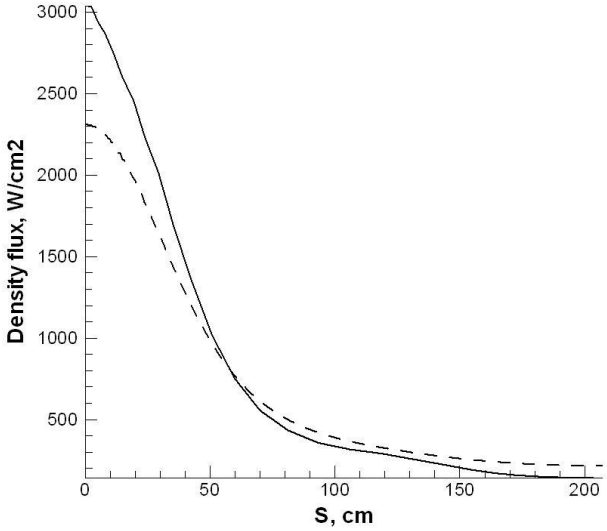

Fig. 16. The flux density to the spherical body, solid curve – RTM, dashed curve - P_1-approximation of SHM, $\kappa = 0.01 cm^{-1}$.

All the rest spectral groups have not been taken into account. The minimum value of absorption coefficient was restricted with value 10^{-2} and 10^{-3} cm^{-1} relatively. On fig. 17 the comparable plot for spectral task is depicted. The relative difference for the front stagnation point is equal 15%, the relative difference for the point 50 cm far from front stagnation point is 60%. Such great difference can be explained small values of absorption coefficient near back stagnation point. The similar calculation was made for absorption coefficient value limitation at 10^{-3} cm^{-1} (fig. 18). The relative difference for the front stagnation point now is 8%, but the difference for the tail part of spherical body now is more sufficient.

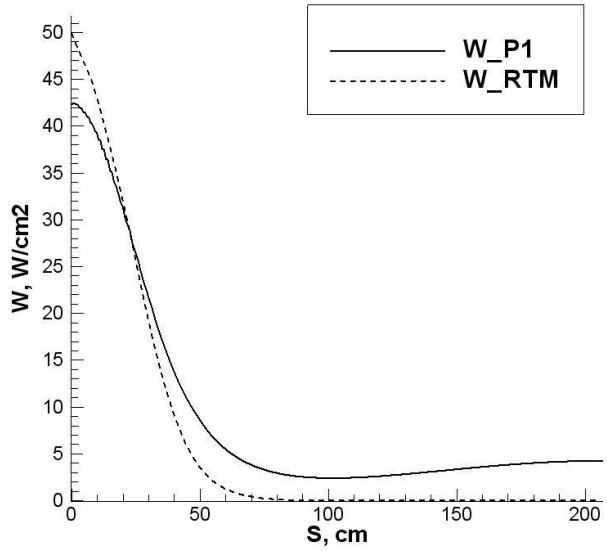

Fig. 17. The flux density, solid curve is P_1-approximation of SHM, dashed curve is RTM. The limitation for absorption coefficient is 10^{-2} cm^{-1}.

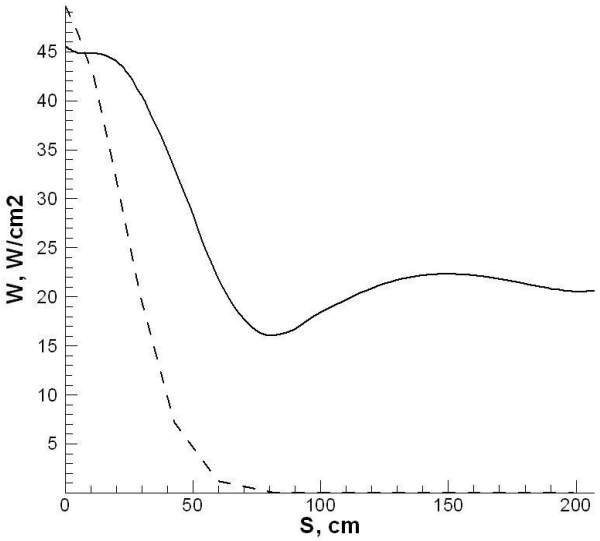

Fig. 18. The flux density to spherical body surface, solid curve is P_1-approximation of SHM, dashed curve is RTM. The limitation for absorption coefficient is 10^{-3} cm^{-1}.

7. CONCLUSION

Results of numerical simulation the heat transfer equation in two-dimensional axisymmetric geometry leads to conclude about peculiarities of application sphere for P_1-approximation of SHM for curvilinear meshes in complex geometry.

The performed calculations of radiative density flux with the linear temperature distribution in the flat layer at different values of the absorption coefficient showed relevancy of this approximation in the range of absorption coefficient $10\text{-}10^{-2}$ cm^{-1}. The maximum of relative difference in the mentioned range of absorption coefficient did not exceed 23%.

Also, the integral and spectral calculation for complex geometry (the flow over the spherical body) is performed. We get the good agreement for integral density flux at absorption coefficient $10\text{-}10^{-1}$ cm^{-1}. The more substantial difference for integral task is observed at absorption coefficient 10^{-2} cm^{-1}. Comparing this result with the calculation for the flat layer at just the same absorption coefficient, one may conclude that the total difference is provided not only because of optically thin medium, but also with the type of geometry.

Taking into account the optical properties of high temperature medium was combined with the "cutting off" the absorption coefficient with the relatively small constant value. The good agreement between flux density predicted by P_1-approximation and RTM for the front stagnation point is obtained. For the back stagnation point the more sufficient difference in flux density value was observed. It is explained with the

much thinner optical medium near back stagnation point.

The essential difference in density flux value for back stagnation point region is also can be explained with the great curvilinearity of the mesh: it is enough to remind that at the same value of absorption coefficient (10^{-2} cm^{-1}) for the flat layer we get quite acceptable difference between P_1-approximation and analytical solution, see fig. 15.

8. ACNOLEGEMENTS

This work was performed with the support of Dmitry Zimin foundation “Dynasty”.

9. REFERENCES

1. Davison B., *Neutron Transport Theory*, Clarendon Press, Oxford, 1958

2. Siegel R., Howell J.R., *Thermal radiation heat transfer*, Hemispere Publishing Corporation, Washington, New York, London, 1971.

3. Surzhikov S.T., *Physico-chemical models for high enthalpy and plasma flows*, von Karman Institute for Fluid Dynamics Lecture series 2002-07, June 2-4, 2002.

4. Greenspan H., Kelber C. N., Okrent D., *Computing methods in reactor physics*, Gordon and Breach Science Publishers, New York, London, Paris, 1972.

5. Fletcher D., Charbonnier J-M., Sarma G.S.B., Magin T., *Radiation modeling and spectral data*, 2002.

6. Lamb H., *Hydrodynamics* 6th ed., Cambridge: Cambridge Univ. Press, 1953, pp. 110-120.

8. Anderson D.A., Tannehill J.C., Pletcher R.H., *Computational Fluid mechanics and heat transfer* Hemisphere Pub. Corp., Vol. 1, pp 297-300, 1984.

9. Andrienko D.A., Surzhikov, S.T., Two dimensional radiation heat transfer to Martian spherical space, *Proceedings of third workshop Radiation of high temperature gases*, Iraklion, Greece, September 30 – October 4, on CD, 2008.

10. Chandrasekhar S., *Radiative transfer*, Dover Publications Inc., New York, 1953.

11. Surzhikov S.T., *Radiative-gasdynamics model of a Martian descent space vehicle*, AIAA 2004-1355, American Institute of Aeronautics and Astronautics, 2004.

12. Surzhikov S.T., *Computing systems for mathematical simulation of selective radiation transfer*, AIAA 2000-2369, 34th Thermophysics Conference, 19-22 June, 2000/ Denver, CO, American Institute of Aeronautics and Astronautics, 2000.